The Journal of Chemical Physics

RESEARCH ARTICLE | MAY 02 2023

Correlated factors for Li-ion migration in ionic conductors with the fcc anion sublattice

Special Collection: Chemical Physics of Electrochemical Energy Materials

Runxin Ouyang ; Zhenming Xu ; Hong Zhu

J. Chem. Phys. 158, 174705 (2023)
https://doi.org/10.1063/5.0140110

AIP Publishing

The Journal of Chemical Physics ARTICLE scitation.org/journal/jcp

Correlated factors for Li-ion migration in ionic conductors with the fcc anion sublattice

Cite as: J. Chem. Phys. 158, 174705 (2023); doi: 10.1063/5.0140110
Submitted: 27 December 2022 • Accepted: 14 April 2023 •
Published Online: 2 May 2023

Runxin Ouyang,[1] Zhenming Xu,[2] and Hong Zhu[1,a)]

AFFILIATIONS

[1] University of Michigan–Shanghai Jiao Tong University Joint Institute, Shanghai Jiao Tong University, 800 Dongchuan Road, Shanghai 200240, China
[2] College of Materials Science and Technology, Nanjing University of Aeronautics and Astronautics, Nanjing 210016, China

Note: This paper is part of the JCP Special Topic on Chemical Physics of Electrochemical Energy Materials.
[a)] **Author to whom correspondence should be addressed:** hong.zhu@sjtu.edu.cn

ABSTRACT

The development of solid-state electrolytes (SSEs) with high lithium ionic conductivities is critical for the realization of all-solid-state Li-ion batteries. Crystal structure distortions, Li polyhedron volumes, and anion charges in SSEs are reported to affect the energy landscapes, and it is paramount to investigate their correlations. Our works uncover the cooperative effect of lithium site distortions, anion charges, and lattice volumes on Li-ion migration energy barrier in superionic conductors of $LiMS_2$ (M = Sc, Ti, V, Cr, Mn, Fe, Co, and Ni) and Li_2MO_3 (M = Sc, Ti, V, Cr, Mn, Fe, Co, and Ni). Combined with the Least Absolute Shrinkage and Selection Operator analyses, the volume and Continuous symmetrical methods (CSMs) of Li tetrahedral (Tet) sites appear to have a larger effect on the manipulation of E_a for Li migration, compared to that of Li octahedral (Oct) sites, which is further confirmed by the results from the face-centered cubic (fcc) anion lattice model. For the Tet–Oct–Tet Li migration path, the CSM (the volume of Li site) has a negative (positive) correlation with E_a, while for the Oct–Tet–Oct Li migration paths, opposite correlations have been observed. The understanding of the correlation between site preference, anion charge, lattice volume, and structural distortion as well as the prediction model of E_a in terms of these three factors, namely, C–V–D model, could be useful for the design of solid-state electrolytes with lower activation energy.

I. INTRODUCTION

The safety problem is the most concerning issue in commercial Li-ion batteries (LIBs) in view of the enormous energy storage devices, such as the electric vehicles.[1] Overcoming the shortages of liquid electrolytes, such as flammability, can be realized by applying high-performance solid-state electrolytes (SSEs), combined with Li metal anodes to construct the all-solid-state lithium-ion batteries (ASSLIBs).[2,3] Achieving the fast conduction of Li ions with the low activation energies and the high Li ionic conductivities at the room temperature is urgent for practical ASSLIBs. Nowadays, a few oxide and sulfide superionic conductors, such as $Li_7La_3Zr_2O_{12}$,[4] $Li_{1+x}Al_xTi_{2-x}(PO_4)_3$,[5] $Li_{10}GeP_2S_{12}$ (LGPS),[6] and $Li_7P_3S_{11}$,[7] have been uncovered as ideal SSE materials. Meanwhile, much research efforts are still being devoted to the better understanding of the fast Li ion diffusion mechanism as well as the design principles, based on which the discovery of new SSE materials could be accelerated.

From the geometric point of view, the body-centered cubic (bcc) anion framework with the Li ions diffusing between two adjacent face-sharing tetrahedral (Tet) sites is reported to be responsible for the high Li conductivity found in LGPS[8] and $Li_7P_3S_{11}$.[9] On the other hand, the distorted Li environments have been also demonstrated important for the fast Li ion diffusions in some Li superionic conductors, such as $LiTi_2(PS_4)_3$ and Li_3MX_6 (M = In, Y, Er, La, X = Cl, Br, I) solid electrolytes.[10–14] For example, the Li sites in $LiTi_2(PS_4)_3$ are heavily distorted, leading to a frustrated energy landscape for Li ions as well as the low activation energies.[11] The incorporation of Br in Li_3OCl is reported to introduce the local structural distortion of Li sites, and the more distorted initial octahedral (Oct) sites and less distorted saddle sites can lead to the lower activation

energy and the enhanced migration entropy.[12] More recently, the superionic oxide conductors with the corner-sharing frameworks, such as $LiGa(SeO_3)_2$, are reported to have the larger distortion of Li sites and the higher lithium conductivities, compared to the counterparts without corner-sharing frameworks.[13] From the perspective of the interaction between Li and anions, it was believed that the small anion charge will be accompanied with fast Li ion diffusions.[14] However, a reverse influence of anion charges on the activation energy for the Li ion diffusing along the Oct–Tet–Oct and Tet–Oct–Tet pathways has been reported, recently. Comprehensively modulating the anion charge and the lattice volume simultaneously seemed to be important to tune the Li occupation sites as well as to reduce the lithium diffusion barrier.[15,16]

Increasing the Li conductivity through reducing the activation energy is so far the most effective and feasible ways, in addition to the optimization of the Li concentrations and prefactors.[15–17] The Li conductivities have been reported to be related to the occupation sites, the site volumes, and the distortions of Li ions, as well as the anion charges. A better understanding of their correlations and the dominant factors for various structural or chemical spaces is still in lack, but of importance.[18,19]

In this work, we explored the correlations between the activation energy and the local environment of the Li site as well as the anion charge, especially for the Li ionic conductors with the face-centered cubic (fcc) anion lattice structures, which compose 29.8% of lithium sulfides and 24.7% of lithium oxides in the Materials Project (MP) database originating from ICSD.[15] For example, the anions of $LiMn_2O_4$, Li_2S, $LiTiS_2$, $LiCoO_2$, Li_2MnO_3, and Li_3YBr_6 form the typical fcc-type frameworks.[15] Moreover, based on our previous study, the Li activation energy in the fcc or hexagonal close-packed (hcp) type anion framework is more sensitive to the site volume as well as the anion charge.[15,16] Two representative material systems with the Li ions occupying the tetrahedral and octahedral sites, respectively, have been considered, namely, the chalcopyrite-structured $LiMS_2$ (M = Sc, Ti, V, Cr, Fe, and Ni) materials[20] and the layered monoclinic-structured Li_2MO_3 (M = Sc, Ti, V, Cr, Mn, Fe, Co, and Ni) materials.[21–23] The volume, distortion, site energy for Li ions at the initial and saddle points, and the anion charges in these two types of materials have been obtained, whose correlations with the activation energies have been discussed and further investigated through the anion lattice model simulations.

II. COMPUTATIONAL METHODOLOGY

Density functional theory (DFT) calculations based on the generalized-gradient approximation (GGA)[24] with the Perdew–Burke–Ernzerhof (PBE)[25] exchange functional and the projector augmented wave (PAW)[26] method were performed by using the Vienna *Ab initio* Simulation Package (VASP) software.[27] The plane wave energy cutoff was set as 500 eV. The convergence criteria in force and energy were set to 0.02 eV/Å and 10^{-7} eV/atom, respectively. The Monkhorst–Pack methods[28] with the $2 \times 2 \times 2$, $4 \times 2 \times 4$ and $4 \times 4 \times 4$ k-point meshes are applied for Brillouin zone sampling of $LiMS_2$, Li_2MnO_3, and fcc-type anion sublattices, respectively. The climbing image nudged elastic band (CI-NEB)[29] calculations were performed for the Li ion migration. For the CI-NEB calculations of Li diffusion in the fcc-type anion sublattice, a 32 anion unit cell with the fixed sulfur (or oxygen) anions was adopted.[9] The anion charges in lithium compounds in this study were calculated by using Bader charge analysis.[30] The structural features considered in this work include the Li site volume and the structural distortion of the Li-anion polyhedrons compared to perfect ones, which were realized through the pymatgen analysis tools.[17,31,33] Continuous symmetrical methods (CSMs) have been used to describe the distortion degree of the local structure of Li ions.[32]

Using the anion framework, the energetics of lithium at the Tet or Oct sites have been evaluated based on the insertion energy of the Li atom (E_i) as follows:

$$E_i = E(\mathrm{Li}X_n) - E(X_n) - E(\mathrm{Li}),$$

where $E(X_n)$, $E(\mathrm{Li}X_n)$, and $E(\mathrm{Li})$ represent the energies for the pure anion (X) framework, the anion framework with one inserted Li ion, and one Li atom in its elemental state, respectively. The relative insertion energy in the deformed fcc anion framework with respect to that in perfect one is defined as $\Delta E_i = E_i^d - E_i^p$. To explore a wider variation of the local structure and charge for the anion framework models, we also applied the electrostatic potential energy calculations based on the Ewald summation method,[33] which is based on the Coulomb–Buckingham model and contains short-range (Li-anion electrostatic attraction) and long-range (Li-cation electrostatic repulsive) interaction, as implemented in the pymatgen code.[31]

III. RESULTS AND DISCUSSION

In the chalcopyrite-structured $LiMS_2$ (M = Sc, Ti, V, Cr, Fe, and Ni) materials, the Li ions migrate from the initial tetrahedral site to the adjacent tetrahedral site through a saddle octahedral site (Tet–Oct–Tet), as shown in Fig. 1(a). For the layered monoclinic-structured Li_2MO_3 (M = Sc, Ti, V, Cr, Mn, Fe, Co, and Ni), the intralayer Li-ion hopping from the initial octahedral site to another octahedral site via a tetrahedral saddle point (Oct–Tet–Oct) with the higher activation energy (E_a) than the interlayer migration is considered, as depicted in Fig. 1(b).[34,35] The activation energy, the anion charge, the volume per anion, and the local structure of Li along the migration paths for $LiMS_2$ and Li_2MO_3 were obtained and depicted in Fig. 2 (see Table S1 in the supplementary material for more details). The specific minimum energy paths (MEPs) for the two materials systems are shown in Fig. S1.

As our previous study elucidated, with the transition metal M changing from Sc to Fe in $LiMS_2$, the volume per S atom (the volume of the compound divided by the number of sulfur atoms) decreases and the anion becomes less negatively charged, which leads to the lower activation energy [shown in Fig. 2(a)].[15] In this work, we further reveal the local structure change of Li sites along the migration path with the transition metal M changing in the ternary lithium sulfides. It is not surprising that the volume of the initial Tet Li site and the volume of the saddle Oct Li site both change linearly with the anion volume as well as the E_a [see Fig. 2(b)]. We also note here that the structural distortions of these Li sites, represented by the CSM values, are negatively correlated with the volumes of the Li sites as well as E_a, as shown in Fig. 2(c). Low E_a in $LiMS_2$ with Tet Li sites results from a larger distortion of Li polyhedron, a smaller volume of the tetrahedral and octahedral sites, and a less negative anion charge.

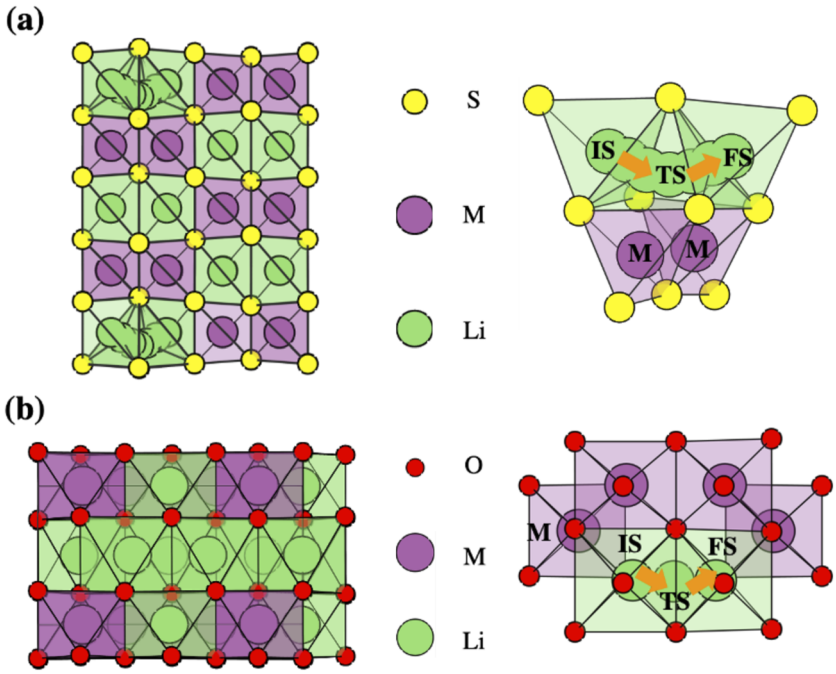

FIG. 1. (a) Crystal structure of $LiMS_2$ (space group *I*42*d* and M = Sc, Ti, V, Cr, Fe, and Ni). Li-ions migrate between two adjacent tetrahedrons through an octahedron. (b) Crystal structure of Li_2MO_3 (space group *C*2/*m* and M = Sc, Ti, V, Cr, Mn, Fe, Co, and Ni). Li-ions migrate between two adjacent octahedrons through a tetrahedron. IS, TS, and FS represent the initial, transition, and final state of the migration for Li ions.

For the intralayer Li-ion migration in layered Li_2MO_3 material, with the transition metal M changing from Sc to Ni, the volume per O atom decreases and the anion becomes less negatively charged, which, however, is accompanied with the higher activation energy [shown in Fig. 2(d)]. Moreover, as depicted in Fig. S13, the electronegativity of the transition metal is increasing from Sc to Ni, while M bader charge in Li_2MO_3, in general, shows a reverse trend. Considering the transition metal elements' electronegativities and electronic configurations, Sc shows a lower bader charge compared to Ti. Such an opposite effect of anion charge and lattice volume on the activation energy for the Li migration along the Oct–Tet–Oct and Tet–Oct–Tet paths agrees with our prior study. Here, we also note that with the volumes of local initial octahedral sites and transition tetrahedral sites of Li_2MO_3 increasing, the Li initial and saddle sites with smaller CSM values become more regular and display smaller E_a, as illustrated in Figs. 2(e) and 2(f). Thus, the low E_a in Li_2MO_3 with Oct Li sites results from a lower distortion degree, the larger volume of the tetrahedral and octahedral sites, and a more negative anion charge. Moreover, the redistributions of Li vibrational density of state (VDOS) where the number of Li vibration modes increases in low-frequency (N_{low}) and high-frequency (N_{high}) is significant to analyze the cation–anion coupling effects. We calculate N_{low}–N_{high}, which characterizes the asymmetric redistribution of VDOS upon the cation and anion coupling, based on allowing or freezing polyanions motions within 300 K AIMD simulations. According to the results in Fig. S14,[36] more positive differences N_{low}–N_{high} lead to lower E_a in $LiMS_2$ (M = Sc, Ti, V, Cr, Fe, and Ni) and Li_2MO_3 (M = Sc, Ti, V, Cr, Mn, Fe, Co, and Ni), which are in agreement with the conclusions reached by Xu *et al.*

To the best of our knowledge, the effects of structural distortions of the Tet and Oct Li sites along the Tet–Oct–Tet and Oct–Tet–Oct migration paths have not been specifically explored before, especially accompanied with the effects of the site volume and anion charge.[11,13] Moreover, from the intuitive thinking, more distorted sites tend to be associated with higher energy in the energy landscape,[11] and in order to modulate the frustrated energy landscape for fast Li-ion migration, distorted sites are apt for the initial positions, while regular sites are desired for transition positions.[12,37] Thus, it is not straightforward to understand why the simultaneous increase in structural distortion for the initial Tet sites and the transition Oct sites for the Tet–Oct–Tet Li migration path (or the simultaneous decrease of structural distortion for the initial Oct sites and the transition Tet sites for the Oct–Tet–Oct Li migration path) reduces E_a. Moreover, it is also not clear that the distortion of which site may have the pivotal roles in manipulating Li energy landscapes and how the charge-volume map on the E_a[15,16] will change in consideration of the structural distortion.

In these two types of ternary Li compounds with the fcc anion lattice structure, the distortion and volume of Li-ion local sites and the anion charge vary upon the non-Li metal elements, which are correlated with each other and strongly related to E_a, as shown in Fig. 2. To better understand their correlations, in addition to the 14 compounds mentioned above, we have also obtained the similar properties for another nine Li compounds with the fcc anion lattice structures (see Table S1) and applied the Least Absolute Shrinkage and Selection Operator (LASSO) method[38–40] to get these factor weights on E_a, as demonstrated in Fig. S2. The performance of model prediction in the LASSO method shows better performance than other regular regressions, as illustrated in Fig. S12. For the 23 fcc-type Li compounds, the LASSO analyses show the greater importance of the volume and CSM of Li Tet sites on E_a compared to those of Li Oct sites. We also note from Fig. S2 that for the Tet–Oct–Tet Li

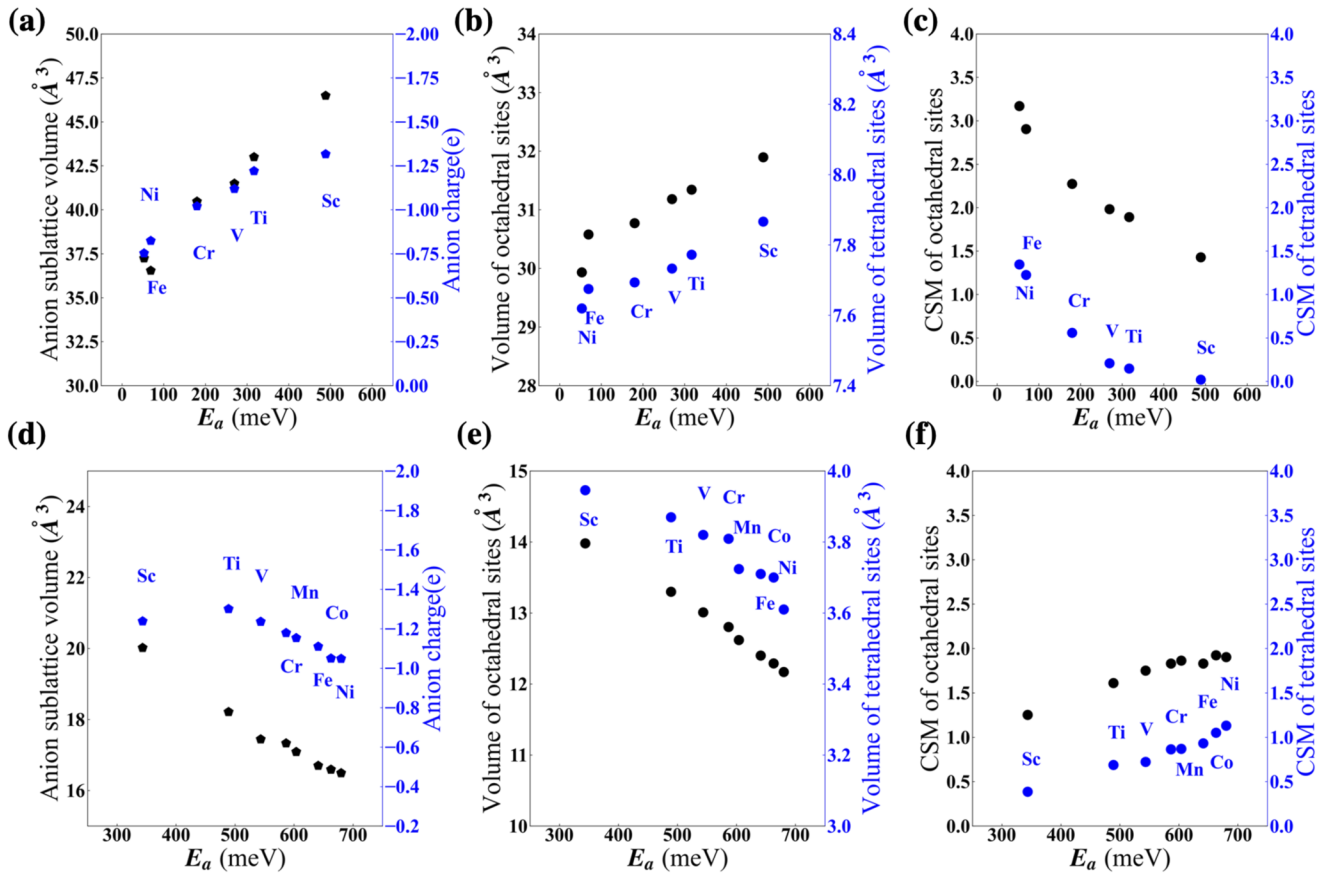

FIG. 2. The lattice volume and anion charge vs E_a for $LiMS_2$ with T-O-T Li migration path (a) and Li_2MO_3 with O-T-O Li migration path (d). The Li volume of tetrahedral and octahedral sites vs E_a for $LiMS_2$ (b) and Li_2MO_3 (e). The CSM of tetrahedral and octahedral Li sites vs E_a for $LiMS_2$ (c) and Li_2MO_3 (f).

migration path, the CSM (the volume of Li site) has a negative (positive) correlation with E_a, while for the Oct–Tet–Oct Li migration paths, opposite correlations have been observed.

To obtain a more comprehensive picture of the correlated effects of site volume, site distortion, and anion charge on the preferred Li occupation site and Li migration barrier for the Li compounds with the fcc anion lattice, we further apply the anion sublattice model with one Li ion.[9,15,16] The anion lattice volume, anion charge, and CSM of the migrating Li polyhedron of the anion model have been varied. The various CSM values of Li sites have been achieved by perturbing a single anion atom of the triangle face between the adjacent Tet and Oct sites along the Li migration path, and the Li site volume and Li ion migration bottleneck area are maintained during the perturbations (see Fig. S3 for more details). Other forms of distortion, such as Bain transformation,[13] has similar effects compared with tune one atom transformation, but specific differences between various forms of distortion are needed further study. The ranges of anion lattice volume, anion charge, and CSM of the Li site considered in this work are based on the distribution of these properties for the Li oxides and sulfides with the fcc anion lattice structure from the Aflow database[41] (as shown in Fig. S4). We note that for the Li sulfides, the S anion lattice volume roughly varies in the range of 20–70 $Å^3$, the S anion charge is in the range of −0.5e to −1.7e, and the CSM values for the Tet and Oct sites are in the range of 0–5 and 0–5, respectively. For the Li oxides, the O anion lattice volume, the O anion charge, and the CSM values for Tet and Oct sites are in the range of 10–40 $Å^3$,[25] −0.5e to −1.7e, 0–5, and 0–5, respectively.

Based on the anion lattice model simulations, we have obtained the Li insertion energy at the Tet and Oct sites and the migration barrier of Li as a function of anion lattice volume, anion charge, and CSM of Li sites for the S and O anion models. Figures S5 and S6 shows the Li insertion energies obtained from the DFT simulations and the E_{wald} summation methods. For clarity, we plotted the heatmaps of the relative Li insertion energy for the distorted site with respect to the perfect site (ΔE_i), the difference of the Li insertion energies at the Tet and Oct sites ($E_i^{tet}-E_i^{oct}$), and the migration barrier of Li (E_a) from the DFT simulations of the S and O anion models in Fig. 3 and Fig. S7, respectively. For simplicity, we focus our discussions on Fig. 3 for the S anion model, while similar observations could[25] be made from Fig. S7 for the O anion model. From Figs. 3(a) and 3(b), it can be found that the relative Li insertion energy at

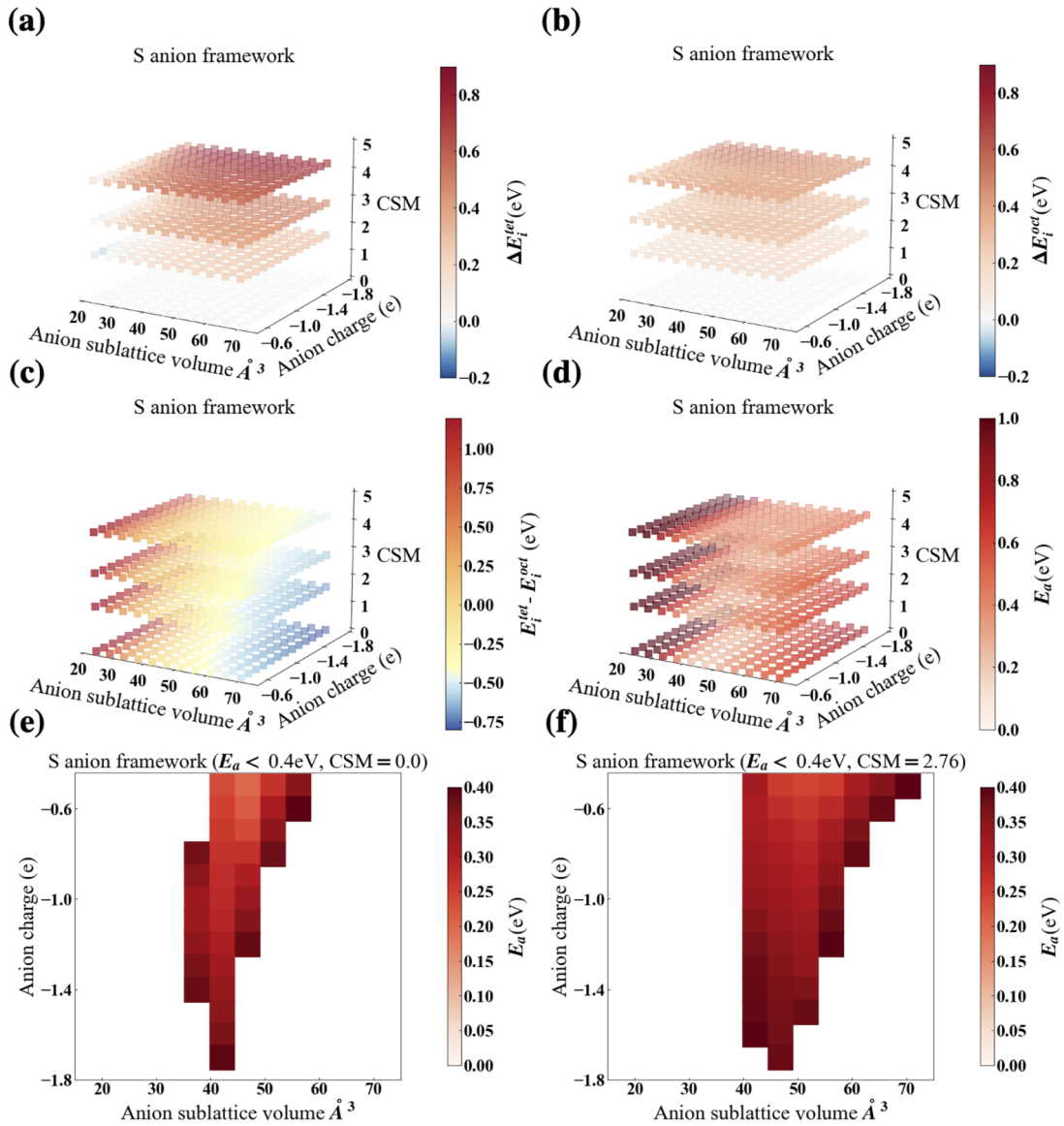

FIG. 3. Heatmaps of (a) relative Li insertion energy for distorted site with respect to the perfect site at Tet sites, ΔE_i^{tet}, (b) relative Li insertion energy for distorted site with respect to the perfect site at Oct sites, ΔE_i^{oct}, (c) Li insertion energy difference between Tet and Oct sites, E_i^{tet}–E_i^{oct}, and (d) Li migration barriers, E_a, as a function of anion sublattice volume, anion charge, and CSM of Li sites in the *fcc*-type sulfur lattice model. The combinations of anion charge and lattice volume leading to Li migration barriers $E_a < 0.4$ eV, (e) for CSM = 0 and (f) CSM = 2.76, respectively, where the data for T–O–T Li migration paths are boxed in blue.

both sites for the S anion model change significantly upon the structural distortion, and how local structural distortion affects ΔE_i is also dependent on the anion sublattice volume and anion charge. Moreover, ΔE_i^{tet} is usually larger than ΔE_i^{oct} for a given anion volume, anion charge, and CSM, suggesting that the Li insertion energy at Tet sites is more sensitive to the structural distortion compared to that at Oct sites. From Fig. 3(c), we note that E_i^{tet}–E_i^{oct}, in general, increases with CSM, decreases with the anion volume, or the more negative anion charge. E_i^{tet}–E_i^{oct} can indicate the most favorable energy sites of Tet vs Oct. E_i^{tet}–$E_i^{oct} < 0$ represents that Li ion tetrahedron sites are energetically more favorable than octahedron sites and Oct Li sites are preferred if E_i^{tet}–$E_i^{oct} > 0$. Thus, to achieve similar insertion energies at the two sites or a smaller absolute value of E_i^{tet}–E_i^{oct}, proper combinations of anion lattice volume, anion charge, and site distortion are required, which are likely to display a low E_a [see Figs. 3(c) and 3(d)]. Figure 3(d) indicates that increasing the CSM could reduce E_a for large anion sublattice volume with Tet Li occupation but increase E_a for small anion sublattice volume

with favored Oct Li occupation, which agree with the findings from Fig. 2.

To better understand their correlated effects on the activation energy for Li diffusion, we further plotted the 2D heatmaps of E_a as a function of anion lattice volume and anion charge for two specific CSM values, 0 and 2.76, where only the cases with the $E_a < 0.4$ eV are shown in Figs. 3(e) and 3(f). It can be found that compared to a perfect Li polyhedron or CSM = 0, a larger local structural distortion of Li sites or larger CSM values could broaden the allowed combinations of anion lattice volume and anion charge for $E_a < 0.4$ eV. Moreover, we can find that for the same anion charge, the allowed anion lattice volume for $E_a < 0.4$ eV increases with the CSM value. More heatmaps showing the combinations of anion charge, anion lattice volume, and CSM values corresponding to different cutoff values of E_a for fcc-type sulfide and oxides can be found in Figs. S8–S10.

In our prior work,[15,16] we have applied only the anion charge (C) and sublattice volume (V) of the Li compounds to predict E_a without considering the local structural distortion, which we call the C–V prediction model. The E_a predicted by the C–V model mostly agreed well with E_a determined from NEB simulations, but some discrepancy was also observed and may benefit from the consideration of structural distortion.[15] Based on the Li migration barrier values in Fig. 3 and Fig. S7, we have applied various regression methods to predict E_a with CSM, anion lattice volume, and anion charge as the three features (see Fig. S11 for more details), and the best achievable MAE for the prediction of E_a for Li diffusion in anion lattice model is ~0.01 eV with the random forest method. Thus, considering the correlated effects of the anion charges (C), anion sublattice volumes (V), and the local distortion of the Li site (D) on the Li diffusion as discussed in details above, we could apply the calculated heatmaps of E_a or the regression model of E_a as a function of C, V, and D as well as the extracted C, V, and D values for a specific fcc-type Li compound to predict its E_a, which is called the C–V–D prediction model. As shown in Fig. 4, the activation energies for Li diffusion predicted based on the C–V–D model for the 23 fcc-type Li compounds in Table S1 agree better with the calculated E_a from NEB simulations, especially for the compounds with large distortions, compared to the C–V model. A detailed comparison could be found in Table S1.

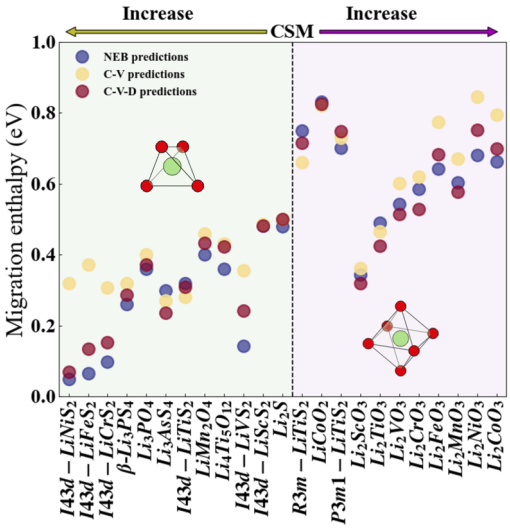

FIG. 4. The migration barriers of Li compounds with the fcc anion lattice structure, predicted from NEB calculations, C–V model, and C–V–D model, where green and purple region represents the Li ion tetrahedron sites and octahedron sites occupations, respectively, which are ranked by the order of CSM from middle to the end.

IV. CONCLUSIONS

In conclusion, the Li-ion migration barrier is correlated with the anion charge, lattice volume, and CSM for $LiMS_2$ and Li_2MO_3 with the fcc type anion lattice structure. Combined with the LASSO analyses, it has been found that the volume and CSM of Li Tet sites has a larger effect on E_a, compared to that of Li Oct sites. From the anion lattice model results, we found that the Li insertion energy at Tet sites is more sensitive to the structural distortion compared to that at Oct sites, and to achieve a low E_a, proper combinations of anion lattice volume, anion charge, and site distortion are required. For the Tet–Oct–Tet Li migration path, the CSM (the volume of Li site) has a negative (positive) correlation with E_a, while for the Oct–Tet–Oct Li migration paths, opposite correlations have been observed. Compared to a perfect Li polyhedron, a larger local structural distortion of Li sites could broaden the allowed anion lattice volume and anion charge combinations for low E_a. The understanding of the correlation between site preference, anion charge, lattice volume, and structural distortion could be useful for the design of solid-state electrolytes with lower activation energy. The C–V–D model proposed in this work can be also applied to the prediction of the Li migration barrier as well as the screening of Li superionic conductors.

SUPPLEMENTARY MATERIAL

See the supplementary material for the complete study of construction and correlation factors for Li-ion migration in the C–V–D model, definition of continuous symmetry measure, and performance of E_a prediction.

ACKNOWLEDGMENTS

This work was supported by the National Natural Science Foundation of China (Grant No. 52072240) and the Materials Genome Initiative Center at Shanghai Jiao Tong University. All simulations were performed at the Shanghai Jiao Tong University High Performance Computing Center.

AUTHOR DECLARATIONS

Conflict of Interest

The authors have no conflicts to disclose.

Author Contributions

H.Z. designed the research and wrote the paper, R.O. performed the DFT calculations and analyzed the data; Z.X. revised the

paper and supply suggestions. All authors discussed and commented on the paper.

Runxin Ouyang: Conceptualization (lead); Data curation (lead); Formal analysis (lead); Funding acquisition (lead); Investigation (equal); Methodology (equal); Validation (lead); Visualization (lead); Writing – original draft (equal); Writing – review & editing (equal). **Zhenming Xu**: Data curation (equal); Methodology (supporting); Writing – original draft (equal); Writing – review & editing (equal). **Hong Zhu**: Funding acquisition (equal); Validation (equal); Writing – review & editing (equal).

DATA AVAILABILITY

The data for building the C–V–D model and predicting E_a by machine learning methods codes are publicly available at Github website, https://github.com/runxin123/C-V-D_model.

REFERENCES

[1] E. Pomerantseva, F. Bonaccorso, X. Feng, Y. Cui, and Y. Gogotsi, "Energy storage: The future enabled by nanomaterials," Science **366**(6468), eaan8285 (2019).

[2] B. Dunn, H. Kamath, and J.-M. Tarascon, "Electrical energy storage for the grid: A battery of choices," Science **334**(6058), 928–935 (2011).

[3] G. Harper, R. Sommerville, E. Kendrick, L. Driscoll, P. Slater, R. Stolkin, A. Walton, P. Christensen, O. Heidrich, S. Lambert, A. Abbott, K. Ryder, L. Gaines, and P. Anderson, "Recycling lithium-ion batteries from electric vehicles," Nature **575**(7781), 75–86 (2019).

[4] R. Murugan, V. Thangadurai, and W. Weppner, "Fast lithium ion conduction in garnet-type $Li_7La_3Zr_2O_{12}$," Angew. Chem., Int. Ed. **46**(41), 7778–7781 (2007).

[5] H. Morimoto, H. Awano, J. Terashima, Y. Shindo, S. Nakanishi, N. Ito, K. Ishikawa, and S. Tobishima, "Preparation of lithium ion conducting solid electrolyte of NASICON-type $Li_{1+x}Al_xTi_{2-x}(PO_4)_3$ (x = 0.3) obtained by using the mechanochemical method and its application as surface modification materials of $LiCoO_2$ cathode for lithium cell," J. Power Sources **240**, 636–643 (2013).

[6] N. Kamaya, K. Homma, Y. Yamakawa, M. Hirayama, R. Kanno, M. Yonemura, T. Kamiyama, Y. Kato, S. Hama, K. Kawamoto, and A. Mitsui, "A lithium superionic conductor," Nat. Mater. **10**(9), 682–686 (2011).

[7] Y. Seino, T. Ota, K. Takada, A. Hayashi, and M. Tatsumisago, "A sulphide lithium super ion conductor is superior to liquid ion conductors for use in rechargeable batteries," Energy Environ. Sci. **7**(2), 627–631 (2014).

[8] F. Liang, Y. Sun, Y. Yuan, J. Huang, M. Hou, and J. Lu, "Designing inorganic electrolytes for solid-state Li-ion batteries: A perspective of LGPS and garnet," Mater. Today **50**, 418–441 (2021).

[9] Y. Wang, W. D. Richards, S. P. Ong, L. J. Miara, J. C. Kim, Y. Mo, and G. Ceder, "Design principles for solid-state lithium superionic conductors," Nat. Mater. **14**(10), 1026 (2015).

[10] N. Adelstein and B. C. Wood, "Role of dynamically frustrated bond disorder in a Li^+ superionic solid electrolyte," Chem. Mater. **28**(20), 7218–7231 (2016).

[11] D. Di Stefano, A. Miglio, K. Robeyns, Y. Filinchuk, M. Lechartier, A. Senyshyn, H. Ishida, S. Spannenberger, D. Prutsch, S. Lunghammer, D. Rettenwander, M. Wilkening, B. Roling, Y. Kato, and G. Hautier, "Superionic diffusion through frustrated energy landscape," Chem **5**(9), 2450–2460 (2019).

[12] R. Chen, Z. Xu, Y. Lin, B. Lv, S.-H. Bo, and H. Zhu, "Influence of structural distortion and lattice dynamics on Li-ion diffusion in $Li_3OCl_{1-x}Br_x$ superionic conductors," ACS Appl. Energy Mater. **4**(3), 2107–2114 (2021).

[13] K. Jun, Y. Sun, Y. Xiao, Y. Zeng, R. Kim, H. Kim, L. J. Miara, D. Im, Y. Wang, and G. Ceder, "Lithium superionic conductors with corner-sharing frameworks," Nat. Mater. **21**(8), 924–931 (2022).

[14] S. P. Culver, A. G. Squires, N. Minafra, C. W. F. Armstrong, T. Krauskopf, F. Böcher, C. Li, B. J. Morgan, and W. G. Zeier, "Evidence for a solid-electrolyte inductive effect in the superionic conductor $Li_{10}Ge_{1-x}Sn_xP_2S_{12}$," J. Am. Chem. Soc. **142**(50), 21210–21219 (2020).

[15] Z. Xu, X. Chen, R. Chen, X. Li, and H. Zhu, "Anion charge and lattice volume dependent lithium ion migration in compounds with *fcc* anion sublattices," npj Comput. Mater. **6**(1), 47 (2020).

[16] Z. Xu and H. Zhu, "Anion charge and lattice volume maps for searching lithium superionic conductors," Chem. Mater. **32**(11), 4618–4626 (2020).

[17] Y. Gao, A. M. Nolan, P. Du, Y. Wu, C. Yang, Q. Chen, Y. Mo, and S.-H. Bo, "Classical and emerging characterization techniques for investigation of ion transport mechanisms in crystalline fast ionic conductors," Chem. Rev. **120**(13), 5954–6008 (2020).

[18] X. He, Q. Bai, Y. Liu, A. M. Nolan, C. Ling, and Y. Mo, "Crystal structural framework of lithium super-ionic conductors," Adv. Energy Mater. **9**(43), 1902078 (2019).

[19] Y. Zhang, X. He, Z. Chen, Q. Bai, A. M. Nolan, C. A. Roberts, D. Banerjee, T. Matsunaga, Y. Mo, and C. Ling, "Unsupervised discovery of solid-state lithium ion conductors," Nat. Commun. **10**(1), 5260 (2019).

[20] Z.-M. Xu, S.-H. Bo, and H. Zhu, "$LiCrS_2$ and $LiMnS_2$ cathodes with extraordinary mixed electron–ion conductivities and favorable interfacial compatibilities with sulfide electrolyte," ACS Appl. Mater. Interfaces **10**(43), 36941–36953 (2018).

[21] M. Y. Yang, S. Kim, K. Kim, W. Cho, J. W. Choi, and Y. S. Nam, "Role of ordered Ni atoms in Li layers for Li-rich layered cathode materials," Adv. Funct. Mater. **27**(35), 1700982 (2017).

[22] P. Xiao, Z. Q. Deng, A. Manthiram, and G. Henkelman, "Calculations of oxygen stability in lithium-rich layered cathodes," J. Phys. Chem. C **116**(44), 23201–23204 (2012).

[23] Y. A. Zulueta, M. T. Nguyen, and J. A. Dawson, "Boosting Li-ion transport in transition-metal-doped Li_2SnO_3," Inorg. Chem. **59**(16), 11841–11846 (2020).

[24] J. Behler and M. Parrinello, "Generalized neural-network representation of high-dimensional potential-energy surfaces," Phys. Rev. Lett. **98**(14), 146401 (2007).

[25] W. Kohn and L. J. Sham, "Self-consistent equations including exchange and correlation effects," Phys. Rev. **140**(4A), A1133–A1138 (1965).

[26] P. E. Blöchl, "Projector augmented-wave method," Phys. Rev. B **50**(24), 17953–17979 (1994).

[27] G. Kresse and D. Joubert, "From ultrasoft pseudopotentials to the projector augmented-wave method," Phys. Rev. B **59**(3), 1758–1775 (1999).

[28] H. J. Monkhorst and J. D. Pack, "Special points for Brillouin-zone integrations," Phys. Rev. B **13**(12), 5188–5192 (1976).

[29] G. Henkelman, B. P. Uberuaga, and H. Jónsson, "A climbing image nudged elastic band method for finding saddle points and minimum energy paths," J. Chem. Phys. **113**(22), 9901–9904 (2000).

[30] M. Yu and D. R. Trinkle, "Accurate and efficient algorithm for bader charge integration," J. Chem. Phys. **134**(6), 064111 (2011).

[31] S. P. Ong, W. D. Richards, A. Jain, G. Hautier, M. Kocher, S. Cholia, D. Gunter, V. L. Chevrier, K. A. Persson, and G. Ceder, "Python materials genomics (pymatgen): A robust, open-source python library for materials analysis," Comput. Mater. Sci. **68**, 314–319 (2013).

[32] D. Waroquiers, X. Gonze, G.-M. Rignanese, C. Welker-Nieuwoudt, F. Rosowski, M. Göbel, S. Schenk, P. Degelmann, R. André, R. Glaum, and G. Hautier, "Statistical analysis of coordination environments in oxides," Chem. Mater. **29**(19), 8346–8360 (2017).

[33] A. Y. Toukmaji and J. A. Board, "Ewald summation techniques in perspective: A survey," Comput. Phys. Commun. **95**(2–3), 73–92 (1996).

[34] Y. Shin, H. Ding, and K. A. Persson, "Revealing the intrinsic Li mobility in the Li_2MnO_3 lithium-excess material," Chem. Mater. **28**(7), 2081–2088 (2016).

[35] R. Xiao, H. Li, and L. Chen, "Density functional investigation on Li_2MnO_3," Chem. Mater. **24**(21), 4242–4251 (2012).

[36]Z. Xu, X. Chen, H. Zhu, and X. Li, "Anharmonic cation–anion coupling dynamics assisted lithium-ion diffusion in sulfide solid electrolytes," Adv. Mater. **34**(49), 2207411 (2022).
[37]K. Kim and D. J. Siegel, "Correlating lattice distortions, ion migration barriers, and stability in solid electrolytes," J. Mater. Chem. A **7**(7), 3216–3227 (2019).
[38]C. Lv, X. Zhou, L. Zhong, C. Yan, M. Srinivasan, Z. W. Seh, C. Liu, H. Pan, S. Li, Y. Wen, and Q. Yan, "Machine learning: An advanced platform for materials development and state prediction in lithium-ion batteries," Adv. Mater. **34**(25), 2101474 (2021).
[39]A. D. Sendek, E. D. Cubuk, E. R. Antoniuk, G. Cheon, Y. Cui, and E. J. Reed, "Machine learning-assisted discovery of solid Li-ion conducting materials," Chem. Mater. **31**(2), 342–352 (2018).
[40]H. Guo, Q. Wang, A. Stuke, A. Urban, and N. Artrith, "Accelerated atomistic modeling of solid-state battery materials with machine learning," Front. Energy Res. **9**, 695902 (2021).
[41]S. Curtarolo, W. Setyawan, S. Wang, J. Xue, K. Yang, R. H. Taylor, L. J. Nelson, G. L. W. Hart, S. Sanvito, M. Buongiorno-Nardelli, N. Mingo, and O. Levy, "AFLOWLIB.ORG: A distributed materials properties repository from high-throughput *ab initio* calculations," Comput. Mater. Sci. **58**, 227–235 (2012).